doi:10.26443/seismica.v5i2.3005

The December 6, 2025 M_w 7.0 earthquake in Yukon, Canada: Assessing routine event data in a remote northern setting

Camille Brillon * [1], **Jeremy M. Gosselin** [1], **Ramin M. H. Dokht** [1], **Andrew J. Schaeffer** [1]

[1]Geological Survey of Canada, Natural Resources Canada, Sidney, BC, Canada

Author contributions: *Conceptualization*: All authors. *Methodology*: Ramin M. H. Dokht, Jeremy M. Gosselin, Camille Brillon. *Software*: Ramin M. H. Dokht, Andrew Schaeffer. *Formal Analysis*: Ramin M. H. Dokht, Jeremy M. Gosselin, Camille Brillon. *Visualization*: Camille Brillon, Jeremy Gosselin.

Abstract The December 6, 2025 M_w 7.0 earthquake in Yukon, Canada, occurred in a remote northern region with sparse seismic coverage. This study evaluates the performance of routine earthquake-related datasets during this sequence, including earthquake catalogues and felt reports, and compares them with a catalogue generated using automated machine-learning detection methods. The enhanced catalogue identifies substantially more events than reviewed databases, particularly Canada's National Earthquake Database. Differences are most pronounced at lower magnitudes and during periods of elevated seismicity immediately following the mainshock. We examine catalogue completeness in response to short-term network saturation and environmental conditions. Despite catalogue limitations, key sequence characteristics, including temporal decay and magnitude–frequency distributions, can be resolved using reviewed databases, albeit with identifiable biases. Community-sourced felt report data provide complementary constraints but remain strongly influenced by population distribution, with comparisons of report density, intensity–distance scaling, and temporal response revealing systematic differences between US and Canadian systems. These results highlight both the value of felt reports for situational awareness and the need for careful interpretation and data assimilation in sparsely populated regions. This study provides important context and practical recommendations for improving Canada's response to significant earthquakes, emphasizing enhanced detection strategies and monitoring in remote, under-served regions.

Production Editor:
Gareth Funning
Handling Editor:
Atalay Ayele Wondem
Copy & Layout Editor:
Sarah Jaye Oliva

Received:
April 14, 2026
Accepted:
August 27, 2026
Published:
November 26, 2026

Non-technical summary On December 6, 2025, a magnitude 7.0 earthquake occurred in a remote part of Yukon, Canada. Because this region has few seismic stations and a small population, it can be challenging to quickly understand how an earthquake sequence is evolving using standard monitoring tools. In this study, we compare the routine datasets available at the time in Canada (such as earthquake catalogues and public felt reports) with a more complete catalogue generated using machine-learning methods. We find that the enhanced catalogue detects many more earthquakes than routine products, especially smaller events and those occurring immediately after the mainshock. This highlights how standard monitoring that is optimized to monitor earthquakes across a geographically large country can miss activity during the most critical early stages of a sequence. Public felt reports, submitted by people who experienced shaking, provide additional useful information. However, our analysis shows that these reports are strongly influenced by where people live. For example, the number of reports, how quickly they are submitted, and the reported shaking levels vary between systems and do not always reflect true ground motion. This means felt reports are helpful for rapid awareness but must be interpreted carefully, especially in sparsely populated regions. Overall, this study provides practical recommendations to improve how Canada monitors and responds to earthquakes, particularly in remote northern areas where data are limited.

1 Introduction

On 6 December 2025, a moment magnitude (M_w) 7.0 earthquake occurred in the remote icefields of southwestern Yukon beneath Mt. King George and the Hubbard Glacier (Figure 1). Although the epicentral region lies within a remote, sparsely populated area of the territory, the earthquake was widely felt across Yukon and neighbouring regions of Alaska, including the territorial capital of Whitehorse approximately 250 km from the epicentre (Natural Resources Canada, 2025). The event represents one of the largest instrumentally recorded earthquakes in Canadian history and the largest onshore crustal earthquake beneath the Canadian landmass since 1946 (Cassidy et al., 2010). Despite the remoteness of the source region, the earthquake generated a rich collection of observations including regional seismic recordings, community-sourced macroseismic felt reports, and a rapidly evolving aftershock sequence.

In this study we examine the earthquake catalogues and felt reports associated with the 6 December 2025 earthquake and its subsequent aftershock sequence,

*Corresponding author: camille.brillon@nrcan-rncan.gc.ca

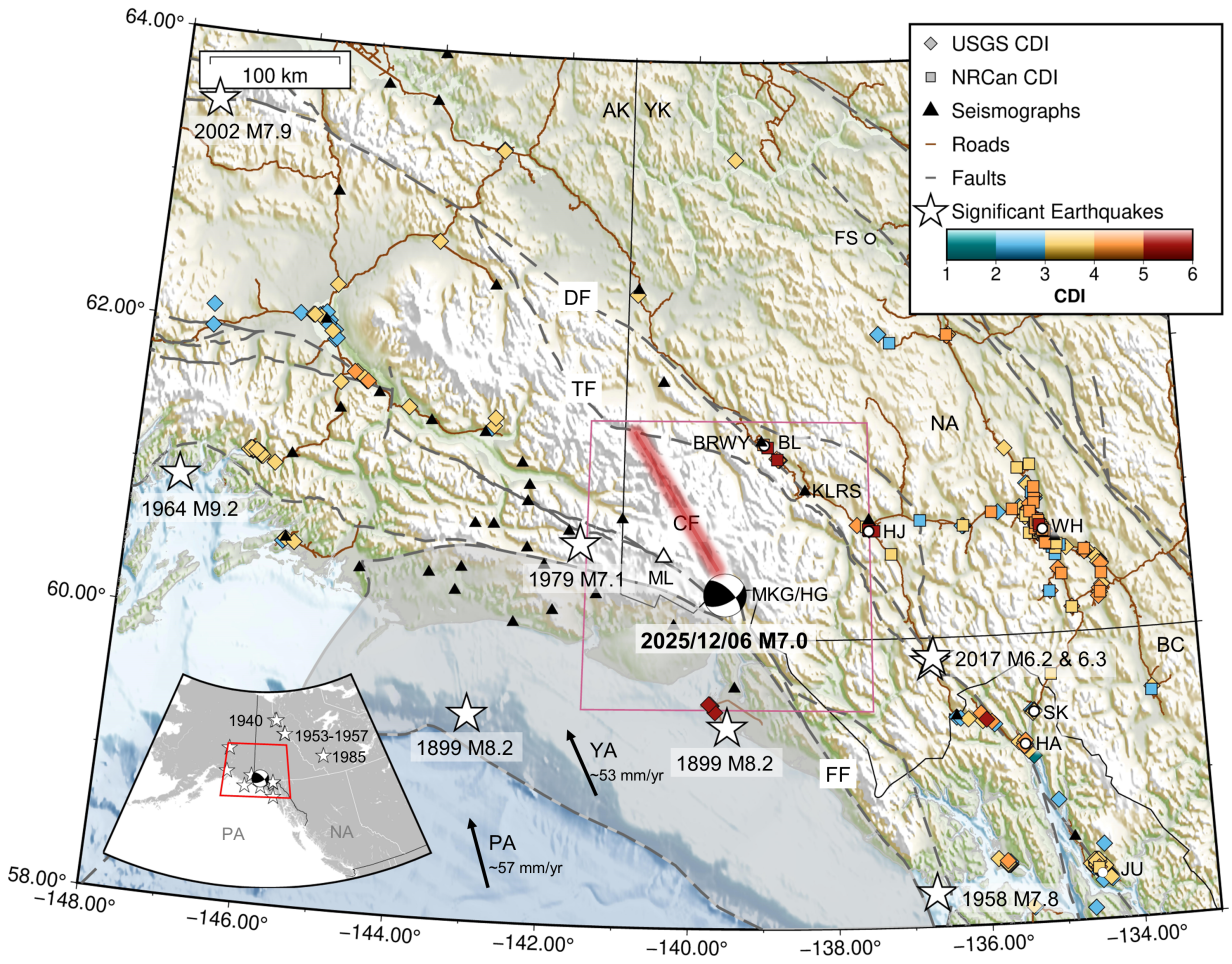

Figure 1 Regional setting and community reporting of the 6 December 2025 M_w 7.0 Yukon earthquake. The epicentre is shown relative to historic significant earthquakes, major tectonic structures, regional population centres (BL=Burwash Landing, HJ=Haines Junction, WH=Whitehorse, FS=Fort Selkirk, SK=Skagway, HA=Haines, JU=Juneau), and infrastructure in Yukon (YK), northern British Columbia (BC), and southeastern Alaska (AK). The event occurred within the complex tectonic boundary zone associated with the oblique collision of the Pacific (PA) and Yakutat (YA) plates with the North American (NA) plate, which drives deformation throughout the St. Elias region (approximately the white areas delineated by the topographic basemap) and along major crustal-scale faults such as the Denali (DF), and Fairweather (FF)–Connector (CF)–Totschunda (TF) fault systems (Yukon Geological Survey, 2021). The mainshock happened beneath Mt. King George and Hubbard Glacier (MKG/HG), in the same region as Canada's highest peak, Mt. Logan (ML). The locations of broadband seismic stations used in this study are shown by black triangles. Aggregated Community Decimal Intensity (CDI) values obtained from NRCan and USGS "Did You Feel It?" (DYFI) reports are also shown. The event faulting mechanism is also shown (U.S. Geological Survey, 2025a). Pink rectangle outlines area shown in Figure S9.

from the two national agencies responsible for disseminating earthquake information in this region, the United States Geological Survey (USGS) and Natural Resources Canada (NRCan). We compile Community Decimal Intensity (CDI) reports from NRCan and USGS "Did You Feel It?" (DYFI) reporting systems. An additional aftershock catalogue, created using machine-learning-based detection and association techniques, was used in the study to provide complementary perspectives on both the physical evolution of the earthquake sequence within the first month following the main event, and the societal experience of shaking across northern communities. The results illustrate how modern seismic monitoring tools and felt intensities can improve understanding of large earthquakes and their aftershocks occurring in sparsely instrumented regions (Bent et al., 2020; Schaeffer et al., 2025). This work also provides important context for future studies of regional tectonics and seismic hazard.

2 Background

Large earthquakes in northwestern Canada have long been documented through observations of shaking, even before the advent of modern seismic instrumentation. Seismicity in Yukon is mostly concentrated in the St. Elias, Richardson, and Mackenzie mountains in southwest, north, and east, respectively (Cassidy and

Bent, 1993; Gosselin et al., 2024; Cassidy and Bent, 2025). Historical records from the mid-19th century indicate that large earthquakes were felt in Yukon hundreds of years ago. A Hudson's Bay Company journal entry from Fort Selkirk (Figure 1), Yukon, describes a strong earthquake on 27 December 1850 that shook buildings for approximately one minute, suggesting an event likely exceeding magnitude 6 and speculated to have originated in the southwest corner of the territory (Jackson, 1990). Almost 50 years later, in 1899, a pair of M_w 8.2 earthquakes resulted in strong shaking and landslides near Hubbard Glacier, 14 m of uplift, and a tsunami in Yakutat Bay (Tarr et al., 1912; U.S. Geological Survey, 2025b). In the modern instrumental era, several earthquakes have produced widespread shaking across the region, including notable felt events such as the 1964 M_w 9.2 earthquake, the 1979 M_s 7.1 earthquake, the 1958 M_w 7.8 earthquake and the May 1, 2017 M_w 6.2 and 6.3 doublet (Figure 1; U.S. Geological Survey, 2025b). The most recent of these events, the 2017 earthquake doublet near the southern segment of the Denali fault at the Alaska–British Columbia border, triggered ground failures, resulted in power outages, and generated 124 felt reports between intensity 3–5 throughout southern Yukon (He et al., 2018; Choi et al., 2021; Natural Resources Canada, 2025). To the north-west, the 2002 M_w 7.9 Denali fault earthquake in Alaska caused strong shaking and infrastructure damage along the Alaska Highway, and was felt throughout much of western Canada (Eberhart-Phillips et al., 2003; Cassidy and Rogers, 2004). At the eastern extent of the territory, the 1940 M_w 6.3 and 6.5 Richardson Mountains earthquakes (Cassidy and Bent, 1993), a series of earthquakes M_w 5.8–6.4 in the Mackenzie Mountains (Cassidy and Bent, 2025), and the 1985 M_w 6.7 and 6.9 Nahanni earthquakes (Wetmiller et al., 1988) were felt across eastern Yukon. This collection of events that have impacted the region highlight the importance of both instrumental monitoring and reported observations of shaking for documenting earthquake effects across northern communities where population density and instrumentation remain relatively sparse. For the 6 December 2025 earthquake examined in this paper, six real-time seismograph stations located within Canadian borders were situated between 115 and 250 km from the epicentre (Figure 1). Although the azimuthal coverage provided by these stations was adequate given the region's geographic constraints, the absence of stations within 100 km of the epicentre limited the availability of near-source instrumental data.

The tectonic setting of southwestern Yukon, which hosted the 2025 event, reflects the ongoing oblique collision of the Yakutat microplate with the North American plate (Gosselin et al., 2024), leading to one of the most actively deforming orogenic regions on Earth in the St. Elias Mountains (Figure 1; Enkelmann et al., 2008), where Canada's highest peak (Mt. Logan) resides. The Yakutat microplate remains mechanically coupled to the Pacific plate, which moves northward along the Queen Charlotte–Fairweather transform system at rates exceeding 50 mm/yr. To the west of the microplate, the Pacific plate subducts beneath Alaska along the Alaska–Aleutian trench. As a result, southwestern Yukon lies within a complex transition between transform motion, subduction, and continental collision where the buoyant Yakutat crust exerts strong control on upper-plate deformation (Plafker, 1987). In this region, plate motion is partitioned between crustal shortening and a network of major right-lateral strike-slip faults that transfer strain into the continental interior (Bruhn et al., 2012).

The 6 December 2025 M_w 7.0 earthquake occurred within this tectonically active zone beneath the heavily glaciated terrain of the St. Elias Mountains. Recent analyses of the sequence indicate that the rupture likely occurred along the southern segment of a hypothesized structural link between the Fairweather and Totschunda fault systems, commonly referred to as the Fairweather–Totschunda Connector fault (CF) (Figure 1; see Finley et al., 2025, and references therein). The existence of this structure has long been inferred from regional tectonic models and patterns of seismicity (e.g., Doser, 2014; Elliott and Freymueller, 2020; Biegel et al., 2024), but it has remained difficult to confirm due to the rough topography, remoteness, and extensive glacial cover of the region. Consequently, the CF has not been clearly mapped at the surface and its role in regional tectonic strain transfer has remained uncertain. Early analyses of the aftershock distribution indicate a northwest–southeast trending rupture extending roughly 50 km from the mainshock epicentre, consistent with the position of an unrecognized segment of the CF (Finley et al., 2025). Early interpretation of mechanisms for the largest aftershocks suggests a complex rupture involving multiple fault strands and possibly, the activation of conjugate structures. The shallow depth of the mainshock and aftershock sequence, generally within the upper ∼10 km of the crust, is also consistent with the relatively thin seismogenic layer inferred for this region (Biegel et al., 2024). These tectonic observations provide important context for interpreting the spatial and temporal patterns of seismicity examined in the following sections.

3 Aftershocks of the December 6, 2025 M_w 7.0 Yukon earthquake

Understanding the spatial and temporal evolution of the 6 December 2025 earthquake sequence requires a catalogue that captures the large number of aftershocks generated during the early stages of the sequence. In remote northern regions such as southwestern Yukon, routine earthquake monitoring relies on relatively sparse seismic networks and operational processing systems that balance rapid reporting with analyst review (Bent et al., 2020; Schaeffer et al., 2025). During large earthquake sequences these workflows often prioritize the largest events, while smaller aftershocks are incorporated later as additional analysis is completed and the rate of larger events decreases. As a result, analyst-reviewed catalogues may temporarily under-represent the full aftershock sequence, particularly in the immediate aftermath of large earthquakes.

In addition to traditional analyst-reviewed earthquake catalogues (e.g., Alaska Earthquake Center, 1987;

Canadian Hazards Information Service, 1985), modern machine-learning detection approaches with targeted application can produce more complete aftershock catalogues that can reveal details of sequence evolution that may otherwise remain unresolved due to network or analyst capabilities (e.g., Mousavi et al., 2020; Jiang et al., 2021). To better characterize the seismicity associated with the 6 December 2025 event, following the first month of the aftershock sequence, we constructed an enhanced earthquake catalogue using machine-learning-based automated detection and association techniques applied to regional seismic network data. This catalogue forms one of the primary datasets presented in this study (Figure 2 and S1).

3.1 Enhanced aftershock catalogue

Continuous seismic waveform data were obtained from the IRIS Data Management Center and include recordings from 39 stations located within approximately 500 km of the mainshock epicentre. These stations combine data from the Alaska Regional Network (AK; Alaska Earthquake Center, 1987), the Alaska Volcano Observatory network (AV; Alaska Volcano Observatory and U.S. Geological Survey, 1988; Dixon et al., 2013), and the Canadian National Seismograph Network (CNSN; Natural Resources Canada, 1975; Bent et al., 2020). Automated detection of seismic events and phase arrivals was performed using the deep-learning-based Earthquake Transformer framework implemented in SeisBench (Mousavi et al., 2020; Woollam et al., 2022). The resulting phase picks were associated into earthquake events using the PyOcto phase association algorithm (Münchmeyer, 2024) and subsequently relocated using the probabilistic NonLinLoc location framework (Lomax et al., 2000). Detailed processing parameters and algorithmic settings used to construct the enhanced catalogue are provided in the Supplementary Material. The goal of creating a machine-learning catalogue is not to replace those produced by national monitoring agencies, but rather to provide a more complete representation of the aftershock sequence in a time-efficient manner by detecting smaller events that may not be included in routine catalogues during periods of intense seismic activity. Automated seismic analysis approaches are particularly valuable in remote regions where station density is limited and analyst resources are necessarily focused on the largest and most significant earthquakes during the early stages of a sequence. The deep learning phase detectors utilized in our workflow are trained on diverse datasets, making the pipeline readily transferable to similar under-instrumented regions without requiring region-specific retraining. The automated detection of low signal-to-noise ratio arrivals remains robust even on isolated stations, though the resolution of phase association and hypocentre location will inherently depend on the station density and azimuthal coverage of the network.

For reference, national earthquake databases in North America are curated and maintained by respective national authoritative agencies, NRCan and the USGS. Earthquakes within Canada are monitored by NRCan via the Canadian National Seismograph Network, and cooperating regional networks, and are archived in the National Earthquake Database (NEDB; Canadian Hazards Information Service, 1985). The NRCan workflow analyses continuous seismic data in near-realtime using automated triggering algorithms within SeisComP seismological software (Helmholtz-Centre Potsdam - GFZ German Research Centre for Geosciences and gempa GmbH, 2008) that identify impulsive seismic arrivals across multiple stations. The earthquake parameters (location and magnitude) resulting from the automatic detection are then reviewed by an analyst prior to being included in the NEDB. Due to operational limitations, not all automatic solutions are reviewed by analysts, and therefore not included in the NEDB. During intense sequences such as the 2025 Yukon earthquake, analyst review is typically prioritized for larger events during the initial response phase, while smaller events may be incorporated later as additional processing is completed.

Comparison between the enhanced catalogue and the NEDB highlights the increased sensitivity of the automated detection workflow (Figure S1). The enhanced catalogue identifies 8,409 earthquakes (Figure 2) between 6 December 2025 and 6 January 2026, compared to 369 events in the NEDB over the same period. All of the events in the NEDB were captured in the enhanced catalogue with average differential distances, origin times and magnitudes of 6.2 km, 0.98 s and -0.23, respectively (Figures S2, S3). It is observed that the largest differences occur for smaller magnitudes. For example, the enhanced catalogue contains 3,979 events with $2.0 \leq M < 2.5$, compared to two in the NRCan catalogue, whereas the two catalogues have almost the identical number of earthquakes (115 and 112, respectively) for events of $3.0 \leq M < 3.5$.

The enhanced catalogue was visually inspected for quality on December 7 and 13, 2025, and these two days were used as a proxy for the remainder of the catalogue. All phases on these 2 days correspond to real events. However, during periods when there are multiple events in a short period of time, some adjacent events share arrivals; for example, the P-wave arrival for one event coincides with the S-wave arrival for the previous event. In the enhanced catalogue there are 143 instances in which the same arrival is associated with two adjacent events. These events are not considered false positives; however, the misidentified arrivals can affect resulting locations and magnitudes. Overall, the enhanced catalogue has epicentral and depth uncertainties of 6.6 km and 1.53 km, respectively (Figure S4). No false events were identified during the visual inspection; however, both days include an event that is likely an icequake. Seven icequakes were identified during the month analysed (U.S. Geological Survey, 2025b) and were likely also identified as earthquakes in the enhanced catalogue. Although numerous landslides are known to have been triggered during this sequence (Finley et al., 2025), the earthquake signals dominate the seismic recordings, resulting in landslide signals being difficult to identify. Landslide signals may obscure the earthquake signals, potentially affecting ar-

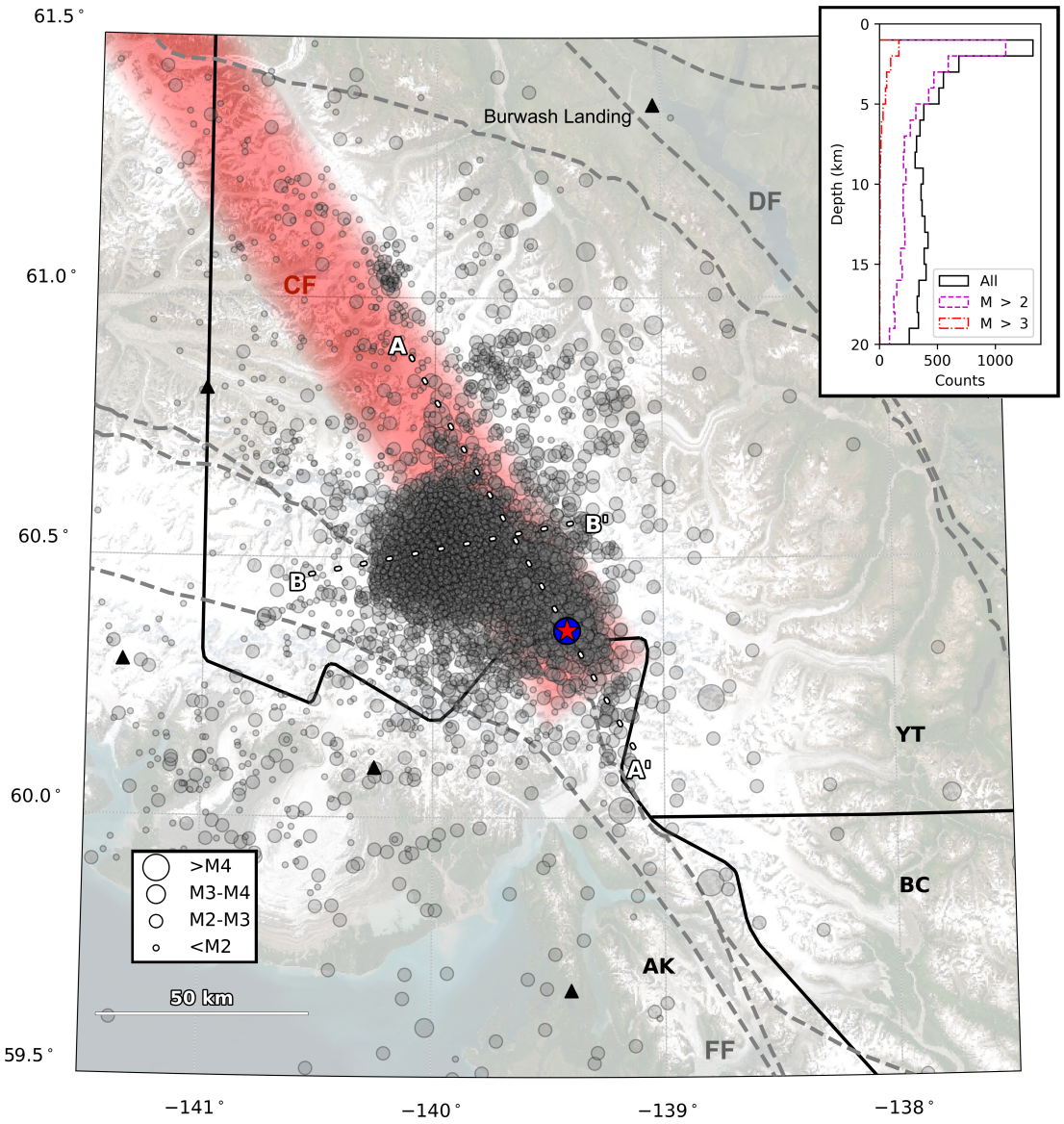

Figure 2 Spatial distribution of earthquakes in the enhanced aftershock catalogue used in this study. Circles represent epicentral locations from the enhanced catalogue, with symbol size scaled by magnitude. The red star marks the epicentre of the 6 December 2025 M_w 7.0 mainshock. The transparent red swath highlights the approximate location and orientation of the hypothesized Connector fault (CF). Grey dashed lines indicate major mapped fault traces in the region, where the Denali fault (DF) and Fairweather fault (FF) are labelled. Solid black lines mark political boundaries between Alaska (AK), Yukon Territory (YT), and British Columbia (BC). The concentration of seismicity surrounding the mainshock outlines the principal aftershock zones (A–A') along the CF, which extends northwest–southeast across the glaciated St. Elias region and (B–B') west of the CF trace. The inset figure shows the distributions of hypocentral depths for the enhanced catalogue. Depth distribution of earthquake epicentres along profiles A–A' and B–B' are included in Figure S5.

rival times and consequently event magnitudes and locations.

Comparison with the USGS catalogue similarly demonstrates the increased sensitivity of the enhanced catalogue. The USGS catalogue contains 3798 events in the first month, with the bulk of the events lying in the magnitude 1.5–2.5 range, and less events than the other two databases above magnitude 3.5 (148 compared to 200 and 225, respectively). We note that in the USGS and NRCan databases, magnitudes are not calculated using identical methods, resulting in some ambiguities at bin edges. We also note that the total number of reviewed and unreviewed events in the NRCan system is similar to the USGS catalogue count, and still significantly less than the enhanced catalogue count. The improved detection capability of the enhanced catalogue is particularly evident during the immediate post-mainshock period and during a secondary burst of seismicity in early January when the number of small aftershocks is highest. These results illustrate how targeted detection approaches can substantially improve aftershock catalogue completeness in remote regions where routine monitoring workflows are optimized for rapid reporting of the

largest events, and are designed to address national monitoring priorities across large geographic areas. For this sequence, the enhanced catalogue was created approximately 6 weeks after the initial earthquake, however, it is possible to run this workflow in near real-time, given that the data are available and the code is optimized for high-performance GPU processing.

3.2 Aftershock sequence observations

The M_w 7.0 mainshock occurred on 6 December 2025 at 20:41 UTC (13:41 Yukon Standard Time) and was reported by Earthquakes Canada (Canadian Hazards Information Service, 1985) at 60.37° N and 139.54° W, near the Alaska–BC border and approximately 50 km southeast of Mt. Logan in the St. Elias Mountains (Figures 1 and 2). The aftershock sequence began immediately following the mainshock, with the earliest aftershock detected 4 minutes and 21 seconds following the mainshock, and continued throughout the study period examined here (6 December 2025 to 6 January 2026). Elevated seismic activity is expected to continue for many months in response to this event.

The spatial distribution of earthquakes in the enhanced catalogue is shown in Figure 2. Seismicity forms a pronounced northwest–southeast trending band extending roughly 50 km across the glaciated St. Elias Mountains. This alignment closely follows the proposed trace of the CF, the Fairweather–Totschunda linking structure, supporting interpretations that the mainshock rupture occurred along this previously hypothesized fault. The densest concentrations of aftershocks occur in two clusters. First, immediately northwest of the mainshock epicentre, aftershocks extend along the inferred CF trace (feature A–A' in Figure 2). Second, an approximately east–west aligned cluster of seismicity is observed west of the CF trace (feature B–B' in Figure 2). These observations are generally consistent with early earthquake relocations discussed in Finley et al. (2025), providing evidence for a more complex rupture of the mainshock. The inset to Figure 2 shows the distribution of hypocentral depths in the enhanced catalogue. The full catalogue shows a broad distribution of reported depths, reflecting the generally poor depth constraints typical for regional seismic networks in this area (see Figure S5). Notably, the catalogue does not contain fixed-depth solutions, which are common in many agency catalogues when depth cannot be well resolved. Depth distributions for subsets of larger events ($M > 2$ and $M > 3$) show a more concentrated distribution at shallow depths. This is consistent with improved depth resolution for higher signal-to-noise events as well as independent evidence that the mainshock rupture occurred in the shallow crust and the shallow seismogenic extent of the crust in this area (Biegel et al., 2024).

Figure 3 illustrates the temporal evolution of the sequence using the enhanced catalogue. The upper panel shows earthquake magnitudes as a function of origin time. The magnitude of completeness (M_c) represents the lowest magnitude above which earthquakes can be reliably detected and included in any statistical analyses (Main, 1996). Several factors influence M_c during an active aftershock sequence. A baseline limitation arises from seismic network geometry, station density, site conditions, instrumentation, and installation quality, which together determine the sensitivity of the network (Lippiello et al., 2012). In addition, short-term increases in M_c commonly occur following large earthquakes when frequent aftershock activity produces overlapping seismic signals and complex coda wavefields that temporarily mask smaller events. This phenomenon, often referred to as short-term aftershock incompleteness (STAI), can significantly reduce the detectability of small earthquakes during the early stages of a sequence and gradually diminishes as seismic activity declines (Kagan, 2004; Lolli and Gasperini, 2006; Figlioli et al., 2024).

The magnitude of completeness is probabilistically estimated within moving 12-hour time windows to illustrate how catalogue completeness evolves through time (Figure 3; Gosselin et al., 2026b). Immediately following the mainshock, the catalogue exhibits an elevated M_c, reflecting the difficulty of detecting small events during periods of intense seismic activity and overlapping waveforms. As the sequence progresses and seismicity rates decline, M_c decreases toward values near $M \sim 2$, indicating improved detection capability as waveform interference becomes less severe. Previous studies have estimated substantially lower completeness levels ($M_c < 1$) in this region during periods of lower seismicity, owing in part to the combined coverage of YUK seismic stations (part of the CNSN network; Meighan et al., 2013) and the temporary EarthScope Transportable Array in Alaska (Busby and Aderhold, 2020; Ruppert and West, 2020). Many of these stations have since been decommissioned or are no longer operational.

Short-term fluctuations in M_c during the sequence also appear to reflect variations in background seismic noise conditions in addition to changes in aftershock productivity (Figures S6 and S7). Power spectral density (PSD) measurements from nearby stations indicate that higher-frequency noise levels (e.g., ∼1 Hz) track the temporal decay of aftershock activity and likely reflect the cumulative seismic energy radiated by the sequence. In contrast, lower-frequency noise levels (e.g., ∼0.1 Hz) show stronger correlations with environmental variables such as wind speed and air temperature, suggesting a greater influence of environmental forcing and surface processes on background, long-period ground motion. Together, these observations highlight that both seismic and environmental factors can influence the detectability of small earthquakes during active sequences.

Figure 3b shows earthquake occurrence rates expressed as counts within 12-hour time bins together with the cumulative number of events detected during the study period. Seismicity rates were highest immediately following the mainshock and declined progressively over subsequent days, consistent with the typical decay behaviour of tectonic aftershock sequences. However, the sequence also exhibits modest deviations from a smooth decay, including a secondary increase in

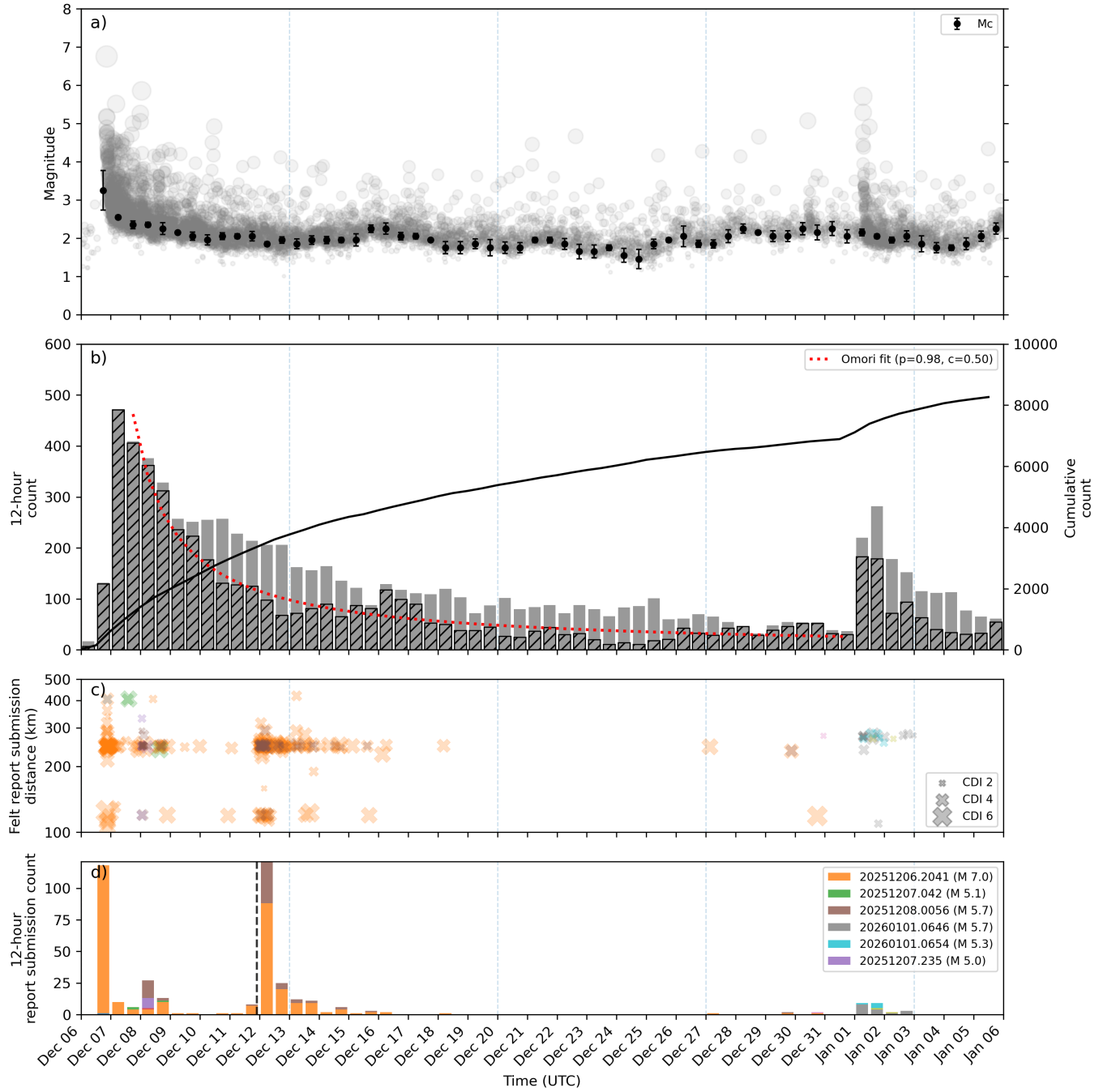

Figure 3 Temporal evolution of seismicity and felt reports following the 6 December 2025 M_w 7.0 Yukon earthquake. (a) Earthquake magnitudes plotted as a function of origin time for events in the enhanced catalogue during the study period. Black symbols with error bars show the probabilistically estimated magnitude of completeness (M_c) calculated within 12-hour moving windows (Gosselin et al., 2026b). (b) Histogram of earthquake occurrence rates in 12-hour bins (grey bars). Hatched bars indicate the subset of events with $M \geq 2.0$, which are used for the Omori analysis to minimize the influence of short-term detection incompleteness. The black curve shows the cumulative number of detected earthquakes. The red dotted line shows the best-fitting modified Omori law fit over the selected time window (6–31 December 2025). (c) Distance of submitted felt reports from the epicentre as a function of submission time. Marker size scales with the Community Decimal Intensity (CDI). Symbols are coloured by event identification number to distinguish reports associated with different earthquakes in the sequence. (d) Number of felt report submissions in 12-hour bins, stacked by event identification number using the same colour scheme as panel (c). The vertical dashed line marks the time of a widely viewed local news story in Whitehorse with direct links to the NRCan earthquake reporting webpage, leading to a resurgence in felt report submissions.

seismicity in early January that reflects renewed clustering following one of the largest aftershocks in the sequence.

The temporal decay of aftershock rates was quantitatively evaluated using a modified Omori law (Ōmori, 1894; Utsu, 1961; Utsu et al., 1995),

$$\lambda(t) = \frac{k}{(t+c)^p},$$

fitted to events with $M \geq 2.0$ in order to minimize the

influence of STAI. Events following the resurgence on 1 January 2026 were also excluded from the fitting window. In this formulation, $\lambda(t)$ represents the aftershock occurrence rate at time t following the mainshock, k describes the productivity of the sequence, p controls the decay rate of seismicity through time, and c represents a time offset that accounts for reduced detectability during the earliest portion of the sequence. The best-fitting parameters ($p = 0.98$, $c = 0.5$ days) indicate a near $1/t$ decay typical of tectonic aftershock sequences, with the non-zero offset parameter reflecting elevated detection thresholds and waveform interference during the first $\sim$12 hours following the mainshock (i.e., even above our $M \geq 2.0$ threshold as can be seen from Figure 3a). Aftershock productivity and decay can be influenced by several factors including mainshock magnitude, regional stress conditions, and the structural complexity of the fault network (Utsu et al., 1995). A more detailed investigation of these controls is beyond the scope of this study but represents a useful direction for future work.

4 Felt intensities of the December 6, 2025 M_w 7.0 Yukon earthquake and aftershocks

4.1 Felt-report datasets

NRCan and the USGS both collect information about the public's experience during earthquakes through online DYFI surveys (Wald et al., 1999). These responses provide valuable macroseismic observations that help characterize shaking intensity, which is particularly beneficial in regions with sparse instrumental coverage. Reports sourced from the community can supplement instrumental ground-motion data, support rapid damage assessments, and provide opportunities for public engagement with earthquake science and emergency response programs (Goltz et al., 2020; Quitoriano and Wald, 2020). Individual responses are typically aggregated to produce CDI values (Dengler and Dewey, 1998), which correspond approximately to the Modified Mercalli Intensity scale describing levels of shaking from I (not felt) to X (extreme) (Wood and Neumann, 1931; Richter, 1958).

Although the overall objectives and outputs of the NRCan and USGS DYFI systems are broadly similar, the two platforms use slightly different questionnaires and aggregation approaches. Because the response formats differ and duplicate submissions to both systems may occur, the datasets cannot be directly merged and are therefore analyzed separately in this study. The location of the earthquake sequence, near the Canada–United States border, resulted in felt reports submitted to both national reporting systems. The observations from this work highlight the importance of inter-agency data assimilation as a future objective for obtaining a comprehensive picture of earthquake intensity during cross-border seismic events.

For the 6 December 2025 Yukon earthquake and aftershock sequence, a total of 408 reports were submitted to NRCan (to 10 events; Natural Resources Canada, 2025) and 1139 reports were submitted to the USGS DYFI system (to 15 events; U.S. Geological Survey, 2026) between 6 December 2025 and 1 February 2026. The majority of reports correspond to the M_w 7.0 mainshock, which alone generated approximately 300 submissions to NRCan and over 1000 submissions to the USGS platform. Of the USGS reports for the mainshock, 276 were from residents of Canadian communities, whereas NRCan received very few reports from US residents.

4.2 Spatial and temporal patterns in felt-report submissions

For the mainshock, the highest CDI values reported to NRCan occur in communities closest to the epicentral region (Figure 4a). In Haines Junction, approximately 123 km east of the epicentre, the maximum reported CDI reached 7.4, while Burwash Landing (approximately 112 km east) recorded a maximum CDI of 5.3. Whitehorse, 250 km away, produced a large number of reports with CDI values exceeding 6, reflecting both the population concentration and possible local geological site effects within the community. However, the spatial coverage of reports within individual communities is uneven and represents the experiences of only a subset of residents, which should be considered when interpreting variations in shaking intensity.

Figure 3 shows the spatial and temporal patterns in NRCan felt-report submissions for the mainshock and aftershocks. Figure S8 similarly shows the USGS felt-report submissions for the mainshock. The majority of reports originate from hypocentral distances of roughly 200–300 km, corresponding to the location of major population centres of Whitehorse, Yukon and Juneau, Alaska relative to the epicentral region (Figure 4). In contrast, relatively few reports originate from the near-source region due to the sparse population in southwestern Yukon. The communities of Burwash Landing and Haines Junction, Yukon, account for the report submissions at approximately 100 km epicentral distance (Figures 3 and 4). Nevertheless, occasional reports at distances exceeding 400 km (and up to $\sim$1000 km in the case of USGS data; Figure S8) indicate that shaking from the mainshock was perceptible over a broad geographic area. The spatial distribution of NRCan-reported shaking intensities for any event in the sequence is illustrated in Figure S9. The mainshock dominates the dataset and, as expected, exhibits systematically higher CDI observations compared to felt aftershocks at equivalent epicentral distances (Figures 4b and S9).

The decay in CDI with increasing epicentral distance is clearly illustrated in Figure S10, which compares NRCan and USGS reports of the mainshock. The USGS DYFI dataset spans a wider range of hypocentral distances, reflecting the broader geographic reach of the USGS reporting system and the presence of larger population centres farther from the epicentre. In contrast, NRCan reports cluster more tightly between approximately 200 and 300 km due to the geographic distribution of communities within Yukon. Despite these differences, both datasets show a general decrease in intensity with increasing distance, accompanied by substan-

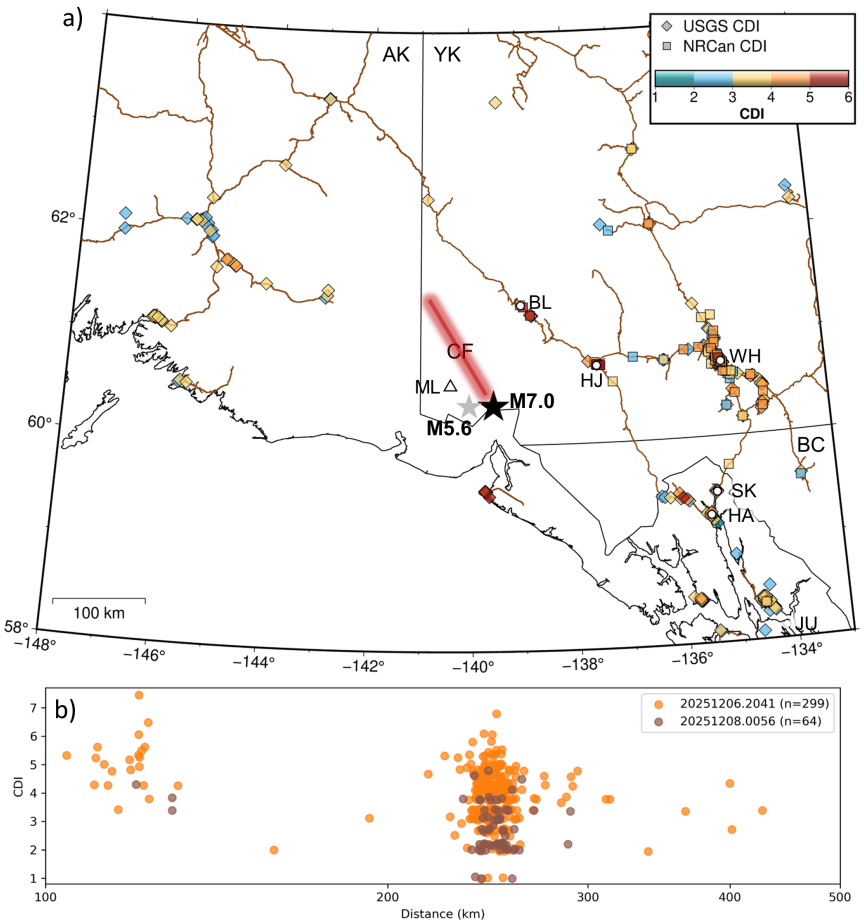

Figure 4 a) Aggregated Community Decimal Intensity reports of the 6 December 2025 M_w 7.0 Yukon earthquake obtained from NRCan (Natural Resources Canada, 2025) and USGS (U.S. Geological Survey, 2026). CDI are shown relative to the location of the mainshock and M_w 5.6 January 1, 2026 aftershock, the proposed Connector Fault (CF, Finley et al. (2025)), Canada's highest peak, Mt. Logan (ML), regional population centres (BL=Burwash Landing, HJ=Haines Junction, WH=Whitehorse, SK=Skagway, HA=Haines, JU=Juneau) and roads (shown by brown lines) in Yukon (YK), northern British Columbia (BC), and southeastern Alaska (AK). Note that squares representing CDI are centered on the location as given in the CDI databases of each agency and scaled for visibility. b) CDI as reported to NRCan as a function of epicentral distance for the 6 December 2025 M_w 7.0 and 1 January 2026 M_w 5.6 Yukon earthquakes. Each marker represents a single report from the NRCan felt-report system, coloured by event identifier, with sample sizes indicated in the legend.

tial variance at comparable distances due to variations in local site conditions, building response, and subjective perception of shaking. We note that the datasets overlap significantly in the 200–300 km epicentral distance range (the majority of these reports correspond to the Whitehorse area) which affords an opportunity to compare the distributions of felt-report outputs. Specifically, the distributions of CDI values within this distance range are quantitatively compared (Figure S7). Two-sample Kolmogorov–Smirnov tests indicate a significant difference between USGS and NRCan CDI distributions (p-values reported in the Supplementary Materials), highlighting systematic differences in reported intensities between platforms at these distances. This points to an important consideration in possible future multi-institution CDI data assimilation. The observed differences between platforms may reflect a combination of population distribution, building stock, local site conditions, reporting methodology, language, and participation bias.

Felt-report submissions show a concentration immediately following the mainshock (Figures 3 and S8). Most reports were submitted to the USGS within the first 24–48 hours. This temporal pattern is consistent with typical DYFI datasets and reflects both the decay of perceptible aftershock activity and the natural decline in public attention following the initial event. Sparse later submissions indicate occasional delayed reports or potential incorrect association of shaking due to subsequent events. However, of the ∼300 reports submitted to NRCan, 132 were submitted in the first 24 hours and the remaining reports were submitted over 3 weeks with the majority of them submitted on December 12. Quantitative comparison of the distribu-

tions of NRCan CDI data for the Whitehorse area before and after 11 December is shown in Figure S11. A two-sample Kolmogorov–Smirnov test indicates no significant difference (p-values reported in the Supplementary Materials), suggesting consistent reporting behaviour over time within the NRCan system. We note that the resurgence in felt-report submissions on 12 December does not coincide with any large aftershocks in the sequence (Figure 3). Instead, we interpret the resurgence to be due to effective communication and outreach via the Yukon Geological Survey, who released a media announcement with direct links to the NRCan felt-report system on 12 December (Yukon Geological Society, 2025). Notably, NRCan discontinued the @CANADAquakes and @CANADAseisme social media notification accounts in early 2024, meaning that no official earthquake notifications were distributed through these widely used channels during the December 2025 sequence. Unlike the NRCan dataset, there is no later temporal resurgence in felt report submissions in the USGS dataset.

Differences between the NRCan and USGS datasets are also evident for several of the largest aftershocks in the sequence. For example, the M_w 5.7 aftershock on 8 December generated 64 reports in the NRCan system but no corresponding submissions in the USGS DYFI database. Most of these reports were submitted from Whitehorse, and most were submitted on 12 December following the Yukon Geological Survey media announcement (Yukon Geological Society, 2025). In contrast, the M_w 5.6 aftershock on 1 January produced 35 reports in the USGS dataset and 16 in the NRCan system, again primarily originating from Whitehorse. Such differences in reporting could point to incorrect event association (particularly for reports submitted on 12 December) or declining reporting participation. Given that these events were reported at distances comparable to other regional communities (e.g., Skagway, Yakutat, and Haines, Alaska), the relative scarcity of reports west and south of the epicentral region may reflect differences in participation rates or differences in perceived shaking (e.g., due to local site conditions). Finally, several smaller events in the sequence are associated with only a few reports in either database, suggesting that some felt reports may be incorrectly associated with nearby events when multiple earthquakes occur within a short period of time.

4.3 Observed shaking and earthquake awareness

To further characterize community experience during the sequence, we examine the detailed content of the felt reports submitted to the NRCan DYFI system for the M_w 7.0 mainshock. Reports were submitted from distances up to approximately 400 km from the epicentre, from single family homes (64%), apartment or condominium buildings (11%) and mobile homes (5%) where respondents described perceptible shaking including swaying motion, rocking or boat-like movement, and horizontal or elliptical ground motion. The reported duration of shaking was typically on the order of several tens of seconds, with a median duration of approximately 30 s. Many respondents described secondary effects such as rattling cabinets, vibrating windows and doors, swaying plants or hanging objects, and objects falling from shelves. These observations are consistent with moderate shaking intensities across populated regions of Yukon and southeastern Alaska; however, intensities do not correlate with geography or building type. Further information about the building, such as number of floors and location of occupants was not included in the DYFI survey at the time of the earthquake.

Responses describing human reactions to the earthquake also provide insight into public awareness and preparedness. The most common response reported by respondents (approximately 45%) was taking no immediate action during the shaking. This likely reflects the relatively moderate intensity experienced in many communities, where shaking was perceived as noticeable but not strongly threatening. The second most frequent response (approximately 29%) involved moving to a doorway. Current earthquake safety guidance recommends *"Drop, Cover, and Hold On"* (DCHO) rather than moving to a doorway, as doorways in modern buildings are not structurally stronger than surrounding walls and provide little protection from falling or flying objects, which account for the majority of earthquake-related injuries (Goltz et al., 2020; Earthquake Country Alliance, 2023; U.S. Geological Survey, 2024). Only a small fraction of respondents (approximately 5%) reported actions consistent with recommended protective behaviour such as DCHO. Although the short duration of shaking may have limited the opportunity to react, the relatively low proportion of respondents reporting recommended safety actions highlights the potential value of increased public education regarding earthquake response in northern Canadian communities.

In addition to regional trends in shaking intensity, the felt-report data also provide preliminary insight into possible local variations in ground motion that may reflect site-response effects within populated areas. Supplementary Figure S13 illustrates the spatial distribution of felt reports within the Whitehorse region at neighbourhood scales for the December 6 mainshock. To preserve respondent privacy, the locations of individual reports were anonymized by introducing small random spatial offsets prior to mapping. Even with this anonymization, the distribution of CDI values suggests noticeable variability in perceived shaking across relatively short distances within the population centre. Such variability likely reflects a combination of local geological conditions, building characteristics, and subjective perception of shaking. These observations highlight the importance of considering local-scale site effects when assessing seismic hazard in northern communities, where detailed site characterization is often limited. Ongoing work by the Geological Survey of Canada and collaborating partners is currently focused on improving characterization of site conditions in several Yukon communities, including Burwash Landing, Haines Junction, and Whitehorse (e.g., Leishman et al., 2024; Byer et al., 2026; Gosselin et al., 2026a).

Instrumental recordings from nearby stations pro-

vide limited constraints on the strongest shaking experienced within communities. The CNSN operates broadband and strong-motion instruments in Burwash Landing (BRWY), Haines Junction, and Whitehorse. An additional autonomous research station is located at the Kluane Lake Research Station (KLRS, Figure 1). During the mainshock, the broadband instruments located at the KLRS (100 km northeast) and BRWY, within Burwash Landing (115 km northeast) went offscale (Figure S12). However, the co-located strong-motion instrument within Burwash Landing recorded a peak ground acceleration (PGA) of 2.4%g and peak ground velocity (PGV) of 3.8 cm/s, which is lower than values typically associated with reported CDI of ∼5 according to empirical intensity–ground-motion relationships (Wald et al., 1999; Worden et al., 2012). In contrast, the instruments serving Haines Junction and Whitehorse are installed on nearby mountaintops rather than within the communities themselves. As a result, these stations recorded shaking levels (PGA 1%g, and .43%g and PGV 1.6 cm/s and 0.95 cm/s, respectively) below that which are associated with the reported intensities highlighting the challenges of comparing instrumental measurements with community-reported intensities when sensors are not located on representative site conditions within populated areas.

5 Conclusions and Recommendations

The 6 December 2025 M_w 7.0 earthquake represents the largest onshore continental earthquake in Canada since 1946 and provides an exceptional opportunity to examine both the seismological evolution of a large earthquake sequence and the societal experience of shaking in a remote northern setting. The enhanced aftershock catalogue compiled in this study reveals a highly active sequence providing strong seismological evidence supporting the existence of the hypothesized CF; the Fairweather–Totschunda connecting structure. Aftershocks define a northwest–southeast trending zone of seismicity approximately 50 km in length, consistent with rupture along the CF. The presence of multiple aftershock spatial clusters suggests a mechanically complex rupture. These observations imply that the CF represents an active through-going structure capable of hosting large earthquakes despite the absence of a clearly mapped surface trace.

Machine-learning-based detection and association methods identify many more events compared to the operational catalogue during the first month of the sequence, while dramatically lowering the completeness threshold of the catalogue. This illustrates how targeted studies employing advanced detection and association methods can significantly improve the characterization of aftershock activity in regions where seismic station coverage and analyst resources are limited. The enhanced catalogue represents a valuable foundation for ongoing and future studies of regional tectonics and seismic hazards.

Community-sourced felt reports provide complementary information regarding the societal impact of the earthquake. The timing and distribution of felt-report submissions highlight the strong influence of outreach and population distribution on macroseismic datasets, with the majority of reports originating from the Whitehorse area and a significant portion of them after a social media post. Comparisons between the NRCan and USGS felt-report databases further suggest that, particularly during the early stages of the sequence, many Canadian respondents may not have been aware of or able to easily locate the NRCan reporting platform. These observations are further complicated by systematic differences between USGS and NRCan CDI estimates at comparable distances from the epicentre, highlighting the need for careful consideration of methodological differences between reporting systems when attempting to assimilate multi-agency macroseismic datasets.

More broadly, the observations presented here underscore the importance and potential benefits to public safety and hazard research of integrating instrumental monitoring, enhanced earthquake detection methods, and community reported observations to improve understanding of earthquakes in sparsely instrumented northern regions. The Yukon earthquake sequence demonstrates that even remote events can generate widespread perceptible shaking and substantial public engagement, providing valuable opportunities for both scientific investigation and communication of earthquake hazards.

Specifically, observations in this paper highlight the need for:

- Integration of machine-learning-based earthquake detection into operational seismic monitoring to lower the magnitude of completeness of earthquake catalogues and provide more consistent and timely characterization of aftershock sequences, improve earthquake hazard research, and reduce operational workload associated with manual review.
- Use of machine-learning-based earthquake catalogues to improve situational awareness, emergency response, and public communication during aftershock sequences, including support for aftershock forecasting and decisions related to ongoing secondary hazards such as landslides.
- Continued improvements to the accessibility and visibility of earthquake reporting platforms, interagency data integration, and public outreach in regions of moderate to high seismic hazard to ensure that community observations can be rapidly incorporated into scientific analyses and situational awareness, and that effective information and guidance can be disseminated during significant earthquake sequences, particularly in regions where regular outreach and public familiarity with earthquake response may be limited.
- Improved understanding of local site response to help refine interpretations of felt-report observations and contribute to more robust seismic hazard assessments for communities across southwestern Yukon.

Looking forward, integrated studies combining seismological observations with geological mapping, geodetic measurements, and investigations of earthquake-induced landslides and cryospheric processes will be essential for improving seismic hazard assessments in northern Canada. Such multidisciplinary approaches are particularly important as climate-driven environmental change continues to modify landscape stability and infrastructure vulnerability across the Arctic and sub-Arctic.

Acknowledgements

The 2025 earthquake sequence occurred primarily on the Traditional Territory of the Kluane First Nation. We thank John Cassidy for valuable early feedback on this work and the anonymous reviewers for their constructive comments. Thank you Vince Quitoriano and David Wald for USGS DYFI data contributions. The software package used to probabilistically estimate catalogue statistical properties (Gosselin et al., 2026b) is available at https://github.com/JMGosselin/BCAUSE.

Data and code availability

Earthquake catalogue data are available from the Natural Resources Canada National Earthquake Database (NEDB) (Canadian Hazards Information Service, 1985). The enhanced earthquake catalogue and associated arrivals are archived on Zenodo and can be accessed at doi: 10.5281/zenodo.19373276. All seismic data were accessed from the NSF NGF data archive operated by EarthScope Consortium (NSF award 2435260), including the following seismic networks (http://ds.iris.edu/mda): (1) the CN (Canadian National Seismograph Network; Natural Resources Canada (1975)); (2) the EO (EON-ROSE; University of Calgary (2018)); (3) the AK (Alaska Geophysical Network; Alaska Earthquake Center (1987)); (4) the AV (Alaska Volcano Observatory; Alaska Volcano Observatory and U.S. Geological Survey (1988)).

The earthquake detection task was performed using the Python packages SeisBench (Münchmeyer et al., 2021) and PyOcto (Yetin, 2023), and event locations were obtained using the NonLinLoc software package (Lomax et al., 2023).

Canadian and US privacy laws prohibit making the intensity data publicly available, and required us to depersonalize reports by reducing the number of significant digits when including reports in figures. Summary data of intensity reports for the earthquakes discussed in this study may be found at Natural Resources Canada (2025) and U.S. Geological Survey (2026). Maps were generated using the Generic Mapping Tools (GMT) version 6 (Wessel et al., 2019).

Competing interests

The authors have no competing interests to declare.

References

Alaska Earthquake Center. Alaska Regional Network, 1987. doi: 10.7914/SN/AK. Seismic network code: AK.

Alaska Volcano Observatory and U.S. Geological Survey. Alaska Volcano Observatory, 1988. doi: 10.7914/SN/AV. Data set.

Bent, A. L., Côté, T. J., Seywerd, H. C., McCormack, D. A., and Coyle, K. A. The Canadian national seismograph network: Upgrade and status. *Seismological Research Letters*, 91(2A):585–592, 2020. doi: 10.1785/0220190202.

Biegel, K. M., Gosselin, J. M., Dettmer, J., Colpron, M., Enkelmann, E., and Caine, J. S. Earthquake relocations delineate discrete fault network and deformation corridor throughout Southeast Alaska and Southwest Yukon. *Tectonics*, 43(5):e2023TC008140, 2024. doi: 10.1029/2023TC008140.

Bruhn, R. L., Sauber, J., Cotton, M. M., Pavlis, T. L., Burgess, E., Ruppert, N., and Forster, R. R. Plate margin deformation and active tectonics along the northern edge of the Yakutat Terrane in the Saint Elias Orogen, Alaska, and Yukon, Canada. *Geosphere*, 8(6): 1384–1407, 2012. doi: 10.1130/GES00807.1.

Busby, R. W. and Aderhold, K. The Alaska transportable array: As built. *Seismological Research Letters*, 91(6):3017–3027, 2020. doi: 10.1785/0220200154.

Byer, J. F., Gosselin, J. M., Dettmer, J., and Gilbert, H. Preliminary investigation of seismic site conditions in Whitehorse (Kwänlin), Yukon, from passive seismic methods. In Stuart, A., Weston, L., and Schultz, S., editors, *Yukon Exploration and Geology 2025*, pages 119–130. Yukon Geological Survey, Government of Yukon, 2026.

Canadian Hazards Information Service. Canadian National Earthquake Database. Natural Resources Canada, 1985. doi: 10.17616/R3TD24. [accessed 8 January 2026].

Cassidy, J., Rogers, G., Lamontagne, M., Halchuk, S., and Adams, J. Canada's Earthquakes: 'The Good, the Bad, and the Ugly'. *Geoscience Canada*, 37(1):1–16, 2010. https://journals.lib.unb.ca/index.php/GC/article/view/15300.

Cassidy, J. F. and Bent, A. L. Source parameters of the 29 May and 5 June, 1940 Richardson Mountains, Yukon Territory, earthquakes. *Bulletin of the Seismological Society of America*, 83(3): 636–659, 1993. doi: 10.1785/BSSA0830030636.

Cassidy, J. F. and Bent, A. L. The MacKenzie Mountains, Northwest Territories, earthquake sequence of 1953 to 1957. *Canadian Journal of Earth Sciences*, 62(4):923–937, 2025. doi: 10.1139/cjes-2024-0132.

Cassidy, J. F. and Rogers, G. C. The Mw 7.9 Denali fault earthquake of 3 November 2002: felt reports and unusual effects across western Canada. *Bulletin of the Seismological Society of America*, 94(6B):S53–S57, 2004. doi: 10.1785/0120040607.

Choi, M., Eaton, D. W., and Enkelmann, E. Is the Eastern Denali fault still active? *Geology*, 49(6):662–666, 2021. doi: 10.1130/g48461.1.

Dengler, L. and Dewey, J. An intensity survey of households affected by the Northridge, California, earthquake of 17 January 1994. *Bulletin of the Seismological Society of America*, 88(2): 441–462, 1998. doi: 10.1785/bssa0880020441.

Dixon, J., Stihler, S., Power, J., Haney, M., Parker, T., Searcy, C., and Prejean, S. Catalog of Earthquake Hypocenters at Alaskan Volcanoes: January 1 through December 31, 2012. Technical Report 789, U.S. Geological Survey, 2013. doi: 10.3133/ds789.

Doser, D. I. Seismicity of southwestern Yukon, Canada, and its relation to slip transfer between the Fairweather and Denali fault systems. *Tectonophysics*, 611:121–129, 2014. doi: 10.1016/j.tecto.2013.11.018.

Earthquake Country Alliance. Drop, Cover, and Hold On, 2023. https://www.earthquakecountry.org/dropcoverholdon/. Accessed 2026.

Eberhart-Phillips, D., Haeussler, P. J., Freymueller, J. T., Frankel, A. D., Rubin, C. M., Craw, P., Ratchkovski, N. A., Anderson, G., Carver, G. A., Crone, A. J., et al. The 2002 Denali fault earthquake, Alaska: A large magnitude, slip-partitioned event. *Science*, 300 (5622):1113–1118, 2003. doi: 10.1126/science.1082703.

Elliott, J. and Freymueller, J. T. A block model of present-day kinematics of Alaska and western Canada. *Journal of Geophysical Research: Solid Earth*, 125(7):e2019JB018378, 2020. doi: 10.1029/2019jb018378.

Enkelmann, E., Garver, J. I., and Pavlis, T. L. Rapid exhumation of ice-covered rocks of the Chugach–St. Elias orogen, Southeast Alaska. *Geology*, 36(12):915–918, 2008. doi: 10.1130/g2252a.1.

Figlioli, A., Vitale, G., Taroni, M., and D'Alessandro, A. Tremors—A software app for the analysis of the completeness magnitude. *Geosciences*, 14(6):149, 2024. doi: 10.3390/geosciences14060149.

Finley, T., Gosselin, J. M., Biegel, K. M., Lipovsky, P. S., Cronmiller, D. C., Schaeffer, A. J., and Dettmer, J. The December 6, 2025 Mw7.0 earthquake in Yukon, Canada: Tectonic significance and observations of ground failure. In Stuart, A., Weston, L. H., and Schultz, S. K., editors, *Yukon Exploration and Geology 2025*, pages 131–148. Yukon Geological Survey, Government of Yukon, Whitehorse, Yukon, Canada, 2025.

Goltz, J. D., Park, H., Quitoriano, V., and Wald, D. J. Human behavioral response in the 2019 Ridgecrest, California, earthquakes: Assessing immediate actions based on data from "Did You Feel It?". *Bulletin of the Seismological Society of America*, 110(4): 1589–1602, 2020. doi: 10.1785/0120200159.

Gosselin, J. M., Biegel, K. M., Dettmer, J., Gilbert, H., Colpron, M., and Enkelmann, E. Crustal stress near the Yakutat microplate collision from probabilistic earthquake focal mechanisms. *Canadian Journal of Earth Sciences*, 62(4):807–820, 2024. doi: 10.1139/cjes-2024-0095.

Gosselin, J. M., Dettmer, J., Lipovsky, P., and Cronmiller, D. Seismic site amplification assessment in the Dakwäkäda (Haines Junction) area of Yukon, Canada, from probabilistic inference of passive seismic measurements. *Canadian Geotechnical Journal*, 63: 1–19, 2026a. doi: 10.1139/cgj-2025-0357.

Gosselin, J. M., Kao, H., Dokht, R. M., and Visser, R. Robust probabilistic estimation of statistical variations in earthquake records: application to induced seismicity in western Canada. *Geophysical Journal International*, 244(3):ggaf450, 2026b. doi: 10.1093/gji/ggaf450.

He, X., Ni, S., Zhang, P., and Freymueller, J. The 1 May 2017 British Columbia-Alaska earthquake doublet and implication for complexity near southern end of Denali fault system. *Geophysical Research Letters*, 45(12):5937–5947, 2018. doi: 10.1029/2018gl078014.

Helmholtz-Centre Potsdam - GFZ German Research Centre for Geosciences and gempa GmbH. The SeisComP seismological software package, 2008. doi: 10.5880/GFZ.2.4.2020.003.

Jackson, L. E. J. Oldest dated earthquake in Yukon Territory, Canada. *Canadian Journal of Earth Sciences*, 27(6):818–819, 1990. doi: 10.1139/e90-084.

Jiang, C., Fang, L., Fan, L., and Li, B. Comparison of the earthquake detection abilities of PhaseNet and EQTransformer with the Yangbi and Maduo earthquakes. *Earthquake Science*, 34(5): 425–435, 2021. doi: 10.29382/eqs-2021-0038.

Kagan, Y. Y. Short-term properties of earthquake catalogs and models of earthquake source. *Bulletin of the Seismological Society of America*, 94(4):1207–1228, 2004. doi: 10.1785/012003098.

Leishman, T., Gosselin, J. M., Dettmer, J., Cassidy, J. F., and Kang, T.-S. Preliminary site characterization for earthquake hazard assessment using ambient vibration techniques in Haines Junction, Yukon (parts of NTS 115A/11, 12, 13, 14). In Weston, L. and Inc., P. R., editors, *Yukon Exploration and Geology Technical Papers 2023*, pages 57–76. Yukon Geological Survey, 2024.

Lippiello, E., Godano, C., and de Arcangelis, L. The earthquake magnitude is influenced by previous seismicity. *Geophysical Research Letters*, 39(5), 2012. doi: 10.1029/2012GL051083.

Lolli, B. and Gasperini, P. Comparing different models of aftershock rate decay: The role of catalog incompleteness in the first times after main shock. *Tectonophysics*, 423(1-4):43–59, 2006. doi: 10.1016/j.tecto.2006.03.025.

Lomax, A., Virieux, J., Volant, P., and Berge-Thierry, C. Probabilistic earthquake location in 3D and layered models: Introduction of a Metropolis-Gibbs method and comparison with linear locations. In *Advances in seismic event location*, pages 101–134. Springer, 2000. doi: 10.1007/978-94-015-9536-0_5.

Lomax, A., Megies, T., Ho, S., Saurel, J.-M., et al. NonLinLoc, 2023. doi: 10.5281/zenodo.8046170.

Main, I. Statistical physics, seismogenesis, and seismic hazard. *Reviews of Geophysics*, 34(4):433–462, 1996. doi: 10.1029/96rg02808.

Meighan, L. N., Cassidy, J. F., Mazzotti, S., and Pavlis, G. L. Microseismicity and tectonics of southwest Yukon Territory, Canada, using a local dense seismic array. *Bulletin of the Seismological Society of America*, 103(6):3341–3346, 2013. doi: 10.1785/0120130068.

Mousavi, S. M., Ellsworth, W. L., Zhu, W., Chuang, L. Y., and Beroza, G. C. Earthquake transformer—an attentive deep-learning model for simultaneous earthquake detection and phase picking. *Nature communications*, 11(1):3952, 2020. doi: 10.1038/s41467-020-17591-w.

Münchmeyer, J. PyOcto: A high-throughput seismic phase associator. *Seismica*, 3(1), 2024. doi: 10.26443/seismica.v3i1.1130.

Münchmeyer, J., Bindi, D., Leser, U., and Tilmann, F. SeisBench: A Toolbox for Machine Learning in Seismology, 2021. https://github.com/seisbench/seisbench. Accessed: April, 2026.

Natural Resources Canada. Canadian National Seismograph Network, 1975. doi: 10.7914/SN/CN. Data set.

Natural Resources Canada. Community Internet Intensity Map. Earthquakes Canada, 2025. https://www.earthquakescanada.nrcan.gc.ca/recent/2025/20251206.2041/dyfi-en.php.

Ōmori, F. On the after-shocks of earthquakes. *The Journal of the College of Science, Imperial University, Japan*, 7(2), 1894.

Plafker, G. Regional geology and petroleum potential of the northern Gulf of Alaska continental margin. In Scholl, D. W., Grantz, A., and Vedder, J. G., editors, *Geology and Resource Potential of the Continental Margin of Western North America and Adjacent Ocean Basins—Beaufort Sea to Baja California*, volume 6 of *Earth Science Series*, pages 229–268. Circum-Pacific Council for Energy and Mineral Resources, Houston, Texas, 1987.

Quitoriano, V. and Wald, D. J. USGS "did you feel it?"—Science and lessons from 20 years of citizen science-based macroseismology. *Frontiers in Earth Science*, 8:120, 2020. doi: 10.3389/feart.2020.00120.

Richter, C. F. Elementary Seismology. *San Francisco*, pages 136–139, 1958.

Ruppert, N. A. and West, M. E. The impact of USArray on earthquake monitoring in Alaska. *Seismological Research Letters*, 91 (2A):601–610, 2020. doi: 10.1785/0220190227.

Schaeffer, A. J., Gosselin, J. M., Audet, P., Colpron, M., Cairns, S.,

and Elliott, B. Western Arctic Regional Network of Seismographs (WARNS): History, challenges and improvements in continuous broadband seismic data recordings in northwestern Canada. In Weston, L. H., Stuart, A., Schultz, S. K., Brubacher, A. D., and Cronmiller, D. C., editors, *Yukon Exploration and Geology Technical Papers 2024*, pages 51–73. Yukon Geological Survey, Whitehorse, Yukon, Canada, 2025.

Tarr, R. S., Martin, L., and Gilbert, G. K. *The Earthquakes at Yakutat Bay, Alaska, in September, 1899*. Number 69 in Professional Paper. U.S. Geological Survey, Washington, D.C., 1912. doi: 10.3133/pp69.

University of Calgary. EON-ROSE, 2018. doi: 10.7914/SN/EO.

U.S. Geological Survey. Earthquake Facts and Earthquake Fantasy, 2024. https://www.usgs.gov/programs/earthquake-hazards/earthquake-facts-earthquake-fantasy. Accessed 2026.

U.S. Geological Survey. M 7.0 – 2025 Hubbard Glacier Earthquake Moment Tensor, 2025a. https://earthquake.usgs.gov/earthquakes/eventpage/us6000rsy1/moment-tensor. [Accessed March 25, 2026].

U.S. Geological Survey. Advanced National Seismic System Comprehensive Earthquake Catalog, 2025b. https://earthquake.usgs.gov/earthquakes. [Accessed January 8, 2026].

U.S. Geological Survey. USGS - Did You Feel It?, 2026. https://earthquake.usgs.gov/earthquakes/eventpage/us6000rsy1/dyfi/intensity. [Accessed February 17, 2026].

Utsu, T. A statistical study on the occurrence of aftershocks. *Geophysical magazine*, 30(4), 1961.

Utsu, T., Ogata, Y., S, R., and Matsu'ura. The centenary of the Omori formula for a decay law of aftershock activity. *Journal of Physics of the Earth*, 43(1):1–33, 1995. doi: 10.4294/jpe1952.43.1.

Wald, D. J., Quitoriano, V., Heaton, T. H., and Kanamori, H. Relationships between peak ground acceleration, peak ground velocity, and modified Mercalli intensity in California. *Earthquake spectra*, 15(3):557–564, 1999. doi: 10.1193/1.1586058.

Wessel, P., Luis, J. F., Uieda, L. a., Scharroo, R., Wobbe, F., Smith, W. H., and Tian, D. The generic mapping tools version 6. *Geochemistry, Geophysics, Geosystems*, 20(11):5556–5564, 2019. doi: 10.1029/2019GC008515.

Wetmiller, R., Horner, R., Hasegawa, H., North, R., Lamontagne, M., Weichert, D., and Evans, S. An analysis of the 1985 Nahanni earthquakes. *Bulletin of the Seismological Society of America*, 78(2):590–616, 1988. doi: 10.1785/BSSA0780020590.

Wood, H. and Neumann, F. Modified Mercalli intensity scale of 1931. *Bulletin of the Seismological Society of America*, 21: 277–283, 1931. doi: 10.1785/bssa0210040277.

Woollam, J., Münchmeyer, J., Tilmann, F., Rietbrock, A., Lange, D., Bornstein, T., Diehl, T., Giunchi, C., Haslinger, F., Jozinović, D., et al. SeisBench—A toolbox for machine learning in seismology. *Seismological Society of America*, 93(3):1695–1709, 2022. doi: 10.1785/0220210324.

Worden, C., Gerstenberger, M., Rhoades, D., and Wald, D. Probabilistic relationships between ground-motion parameters and modified Mercalli intensity in California. *Bulletin of the Seismological Society of America*, 102(1):204–221, 2012. doi: 10.1785/0120110156.

Yetin, A. M. PyOcto: A High-Throughput Seismic Phase Associator, 2023. https://github.com/yetinam/pyocto. Accessed: April, 2026.

Yukon Geological Society. Facebook Post, 2025. https://www.facebook.com/share/p/1CZm4ktDBj/. [Accessed: February 17, 2026].

Yukon Geological Survey. Major Faults. Government of Yukon, 2021. https://open.yukon.ca/data/major-faults.

The article *The December 6, 2025 M_w 7.0 earthquake in Yukon, Canada: Assessing routine event data in a remote northern setting* © 2026 His Majesty the King in Right of Canada, as represented by the Minister of Natural Resources. Non-Commercial Reproduction. Permission to reproduce Government of Canada works, in part or in whole, and by any means, for personal or public non-commercial purposes, or for cost-recovery purposes, is not required, unless otherwise specified in the material you wish to reproduce. Please see NRCan's terms of use for commercial reproduction: https://natural-resources.canada.ca/terms-and-conditions/10847.